Cation role in the thermal properties of layered materials $M^{1+}M^{3+}P_2(S, Se)_6$ (M^{1+} = Cu, Ag; M^{3+} = In, Bi)

V. Liubachko,[1,2] A. Oleaga,[1,*] A. Salazar,[1] A. Kohutych,[2] K. Glukhov,[2] A. Pogodin,[2] and Yu. Vysochanskii[2]

[1]*Departamento de Física Aplicada I, Escuela de Ingeniería de Bilbao, UPV/EHU, Plaza Ing. Torres Quevedo 1, 48013 Bilbao, Spain*

[2]*Institute for Solid State Physics and Chemistry, Uzhgorod University, 88000 Uzhgorod, Ukraine*

(Received 21 June 2019; revised manuscript received 16 September 2019; published 21 October 2019)

Thermal properties (thermal diffusivity, heat capacity, and thermal conductivity) have been retrieved for the layered compounds $Cu_{1-x}Ag_xInP_2(S, Se)_6$, $AgBiP_2(S, Se)_6$, and $CuBiP_2Se_6$ in the temperature range 30–350 K, using single crystals. A complete explanation of the thermal properties as ions are substituted has been developed, showing the role played by disorder, electronic levels hybridization, ion coordination, or size on the second-order Jahn-Teller effect. The evolution of the thermal diffusivity and the thermal conductivity with temperature has shown, on the one hand, strong thermal anisotropies and, on the other hand, that heat is effectively transferred by phonons, with some of the compounds (especially those with Bi) presenting very low values due to the enhancement of phonon scattering events, expressing a strong anharmonic behavior, which is justified in detail, case by case, on the basis of interactions among optical and acoustic phonon branches as well as the presence of electron lone pairs. This broad study opens up the possibility of designing new materials for applications where a low thermal conductivity is essential.

DOI: 10.1103/PhysRevMaterials.3.104415

I. INTRODUCTION

The big family of metal thio- and selenophosphates compounds is attracting huge interest from the scientific community as multifunctional van der Waals Layered materials, searching for the development of 2D-materials with correlated magnetic, structural and ferroelectric properties [1,2]. In particular, layered crystals of hexachalcogenohypodiphostates with the general formula $M^{1+}M^{3+}P_2X_6$ (M = metal cations, X = S, Se) are promising candidates as they are semiconductors with an intermediate bandgap suitable for new electronic applications, while they also exhibit (anti)ferroelectric properties or/and (anti)ferromagnetic, or/and piezoelectric [1,3–7]. The knowledge of their thermal properties, alongside with the ferroelectric ones, is necessary for their applications in technological devices, including the possibility of finding compositions with very low thermal conductivity, as it has also been shown in another family of phosporous chalcogenide crystals [8].

In this work, we are presenting a complete study of the compounds with M^{1+} = Cu, Ag, M^{3+} = In, Bi and X = S, Se in the form $Cu_{1-x}Ag_xInP_2(S, Se)_6$, with x = 0, 0.1, and 1, $AgBiP_2(S, Se)_6$, and $CuBiP_2Se_6$. Due to their layered character, the anisotropic thermal properties (thermal diffusivity and thermal conductivity) will be evaluated in two directions: one contained in the layers and another one perpendicular to them. Thermal diffusivity will be measured with a high-resolution technique, paying special attention to the presence or absence of any kind of ferroelectric ordering which should be appreciated as some kind of singularity on the thermal diffusivity curves as a function of temperature; heat capacity will be calculated from first principles theories and, combining both physical properties, thermal conductivity will be extracted.

The scope of available information in literature on these compounds is quite varied. Though all compounds $M^{1+}M^{3+}P_2(S, Se)_6$ present an anion sublattice $[P_2X_6]^{4-}$ (X = S, Se) within each lamella of the layered crystal, they crystallize in different space groups [1,9–14], which has a strong influence on their physical properties. Concerning ferroelectricity, $CuInP_2S_6$ has a first-order ferrielectric transition, $CuInP_2Se_6$ presents a ferrielectric one, $AgBiP_2Se_6$ is in an antiferroelectric state in all the temperature range studied so far (110–350 K), $CuBiP_2Se_6$ has an antiferroelectric transition and in the rest either no polar phases have ben found ($AgInP_2S_6$, $AgInP_2Se_6$) or it is unclear ($AgBiP_2S_6$).

The transition in $CuInP_2(S, Se)_6$ is linked to the local dynamic hopping of Cu^+ ions [9,15] which induces a second-order Jahn-Teller (SOJT) effect, whose presence or absence is severely dependent on the covalency of the bonds and the hybridization of the s and d orbitals of the M^{1+} cation. The latter is more efficient in silver doped compounds in the paraelectric phase, leading to a bigger covalency of the Ag-$[P_2S_6]$ bonds [13]. Besides, the bigger size of Ag ions compared to Cu makes more difficult to freeze the hopping motion of the former, leading to the absence of ferroelectric properties in $AgInP_2(S, Se)_6$ [16]. The main difference between $CuInP_2Se_6$ and $CuBiP_2Se_6$ lies on the fact that Bi s^2 lone pair is stereochemically expressed and, in the ordered phase, the Bi ions are displaced in the opposite direction as Cu ones [12], creating a ferrielectric state.

Finally, though $AgBiP_2Se_6$ has many structural similarities with $CuBiP_2Se_6$ in the ordered phase [12], the lone pair of bismuth is not stereochemically expressed. The origin of its

*alberto.oleaga@ehu.es

antiferroelectric behavior is the ordered displacement of the Ag ions along the *c* axis. In $AgBiP_2S_6$ a study on ultrasonic velocity found a small singularity at about 220 K which the authors identified as a phase transition [17]; it is worth noting that the crystal structure of $AgBiP_2S_6$ is very different from $AgBiP_2Se_6$ due to several reasons: a different coordination environment for Bi, the smaller size of S compared to Se and a tendency to stereochemically express the lone pair [12]. Besides the cited studies, there are also some scarce studies on electrical and ultrasonic properties [17–26] as well as on thermal properties [27,28] but not too many.

The purpose of this paper is to shed light on the role that the different cations play in $M^{1+}M^{3+}P_2(S, Se)_6$ (M^{1+} = Cu, Ag; M^{3+} = In, Bi) on the thermal transport properties, paying special attention to the anharmonic mechanisms which can lead to a substantial reduction of the thermal conductivity. To this end, we have gathered previous measurements of thermal diffusivity on $CuInP_2(S, Se)_6$, $AgInP_2(S, Se)_6$, $CuBiP_2Se_6$ [29,30] and are presenting new measurements for $Cu_{0.9}Ag_{0.1}InP_2(S, Se)_6$, $AgBiP_2(S, Se)_6$.

II. SAMPLES AND EXPERIMENTAL TECHNIQUES

Single crystals of ternary hexachalcohipodiphosphates $Cu_{1-x}Ag_xInP_2(S, Se)_6$ with $x = 0$, 0.1, and 1, $AgBiP_2(S, Se)_6$ and $CuBiP_2Se_6$ were grown for this study [11,14,31–33]. Another logical candidate to grow and study would be $CuBiP_2S_6$ but, for the time being, it is impossible to grow. From the single crystal boules, samples were cut and prepared as thin plane-parallel slabs whose surfaces are either parallel to the layers or perpendicular to them, obtaining two orientations per sample in order to study possible thermal anisotropies.

A high-resolution *ac* photopyroelectric calorimeter in the back configuration has been used to measure thermal diffusivity *D* as a function of temperature, where it is measured in the direction perpendicular to the surface of the sample. The details of the technique as well as of the experimental setup can be found elsewhere [34]. The selected temperature range has been 30–350 K (seldom used in literature) in order to check the possible ferroelectric orderings in a very broad temperature range. Very low heating and cooling rates are used when verifying the possible hysteresis of the transitions, even down to 10 mK/min for particular cases.

The heat capacity *C* of all considered crystals has been calculated by means of ABINIT software code [35] utilizing the density functional theory approach [36]. The exchange-correlation interaction was taken into account within the generalized gradients approximation (GGA) [37]. Also, the dispersion (DFT-D) correction by Grimme [38] has been used to take into account the van der Waals interaction between the layers of the considered crystals. The cutoff energy for plane-wave basis set was restricted by 850 eV. The $3 \times 3 \times 2$ mesh of the special k-points for wavefunctions expansion was generated according to Monkhorst–Pack scheme [39]. The density functional perturbation theory (DFPT), was used for the calculation of the lattice dynamics [40] and for the estimation of the specific heat within the harmonic approximation [41]. The symmetry of the primitive cells was preserved while optimizing the geometry. Once the phonon spectra is calculated, the corresponding density of phonon states can be obtained, and then the heat capacity [42].

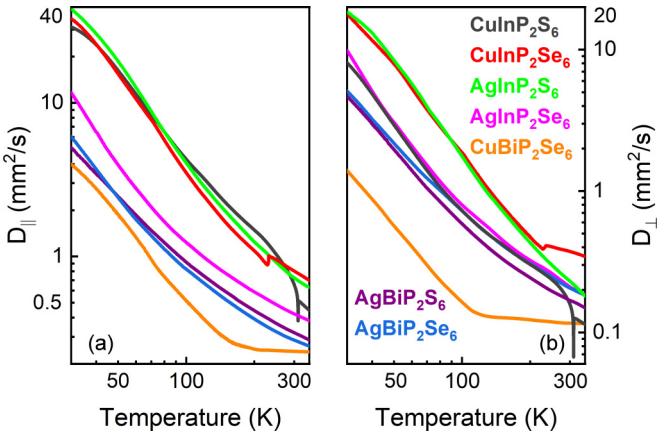

FIG. 1. Thermal diffusivity measured as a function of temperature for all compounds, measured along the layers (a) and perpendicular to them (b).

The values of C_v for all considered crystals were obtained for low-temperature structures because the *ab initio* simulations were performed at $T = 0$ limit. The temperature dependence of heat capacity modeled in such approach reproduces only the regular behavior of C_v and doesn't include peculiar features at the phase transition temperature; nevertheless, these dependencies are sufficient for the estimation of the thermal conductivity in regions beyond the transition.

The combination of the measured thermal diffusivity and the calculated heat capacity allows retrieving the thermal conductivity using the following equation:

$$k = C\,D, \tag{1}$$

where the regions where there is any phase transition have been removed from *D* as only the background heat capacity has been calculated.

III. RESULTS AND DISCUSSION

A. Thermal diffusivity and phase transitions

Figure 1 shows the thermal diffusivity of the compounds in the range 30–350 K in a log-log scale. In every case, both orientations have been studied and labeled as ∥ for the thermal diffusivity measured along the layers and as ⊥ when it is measured perpendicular to them. There are common trends shared by all the samples: At high temperature the values are small, typical for insulating materials, where heat is mainly transferred by phonons. As the temperature decreases there is a monotonic increase in the value of *D* (as the phonon mean-free path increases) which quickly grows at low temperature, starting at very close temperatures among the samples. This sudden growth should start at temperatures close to the Debye temperature, whose value is known only for $CuInP_2Se_6$ (75.9 K) [28] and which coincides well with the experiment.

Thermal anisotropy is present in all compounds: heat is much more easily transferred along the layers, as proved by the values of *D* being between twice and four times higher along the layers than perpendicular to them. This

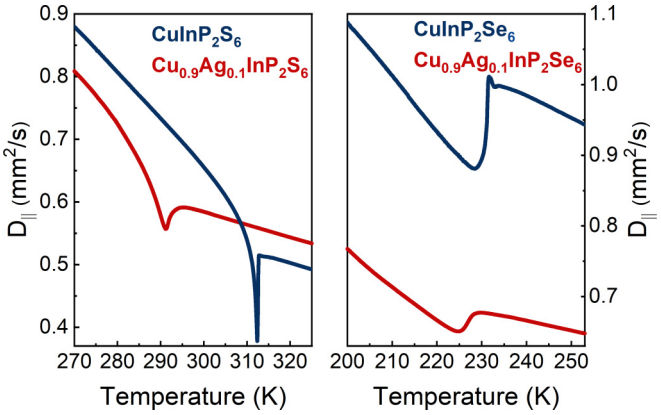

FIG. 2. Phase transitions evolution while introducing Ag : $CuInP_2S_6$, $Cu_{0.9}Ag_{0.1}InP_2S_6$, $CuInP_2Se_6$, $Cu_{0.9}Ag_{0.1}InP_2Se_6$. The thermal diffusivities are measured along the layers.

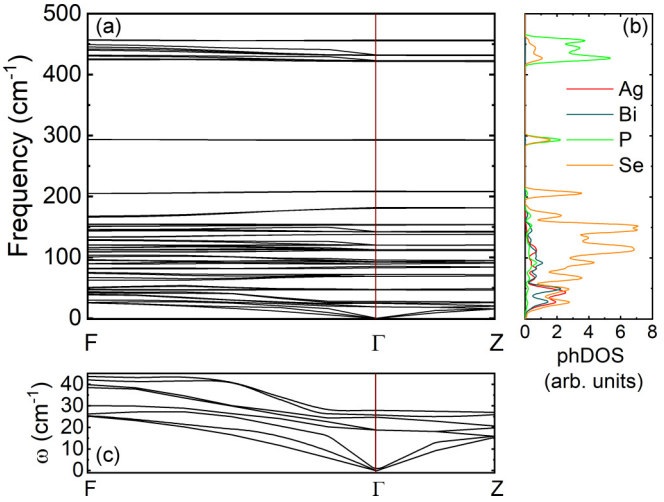

FIG. 3. (a) Calculated phonon spectrum and (b) phonon density of states for $AgBiP_2Se_6$ crystal; panel (c) shows the detail of the phonon spectrum at low frequencies.

anisotropic behavior is commonly found in 2D materials, such as graphene, graphyne, borophene, MoS_2, $ZrTe_5$, or carbon nanotubes [43–47].

Concerning phase transitions, these are marked on the thermal diffusivity curves as dips of different sharpness but only in some compounds, confirming the transitions in $CuInP_2S_6$ and $CuInP_2Se_6$ and the full ferroelectric frustration in $AgInP_2S_6$ and $AgInP_2Se_6$ down to 30 K (the lowest temperature studied for these compounds in literature was 110 K) [23]. Figure 2 shows how this frustration is developed in $Cu_{0.9}Ag_{0.1}InP_2(S, Se)_6$, with smeared transitions and shifts to lower temperatures. The introduction of Bi instead of In has the general consequence of making heat transfer more difficult, as the values of D in all directions are smaller than the corresponding with In. Neither $AgBiP_2Se_6$ nor $AgBiP_2S_6$ shows any singularity in the curves, confirming the absence of a paraelectric phase in the former up to 350 K and establishing the ferroelectric frustration in the latter down to 30 K.

B. Heat capacity

The molar heat capacity has been calculated as explained in Sec. II for all samples. Figure 3 shows, as an example, the calculated phonon spectrum and phonon density of states (phDOS) for the case of $AgBiP_2Se_6$, while Fig. 4(a) contains the calculated specific heats for all samples. The only composition for which heat capacity has been measured in literature is $CuInP_2Se_6$ [28] and Fig. 4(b) contains the comparison with the calculated one. The agreement of the background heat capacity is very good, confirming the reliability of the calculations.

C. Thermal conductivity

Figure 5 shows the thermal conductivity for the compounds studied in this work, calculated using Eq. (1), for both orientations. In order to analyze their temperature dependency, the Debye temperatures for each compound have been calculated from the phonon dispersion spectra as

$$T_D = \frac{\hbar\omega_D}{k_B}, \tag{2}$$

where $\hbar$ is the reduced Plank constant, k_B the Boltzmann constant and ω_D the Debye frequency, for which the lowest optical branch has been taken, and they are shown in Table I. The temperature dependence of the lattice thermal conductivity approximately follows a $1/T$ law in a region which, for each compound, is placed near the Debye temperature and a little above (Fig. 5). At higher temperatures κ (T) dependence reflects the temperature dependence of the sound velocity and heat capacity. This behavior is valid only in the regime where the phonon mean-free path exceeds the interatomic distance. In $CuBiP_2Se_6$ compound the lattice thermal conductivity has already reached its lowest value of approximately $0.20\,Wm^{-1}\,K^{-1}$ near 100 K, surely because the phonon mean-free path has already decreased to the interatomic distance and cannot decrease further.

Near the Debye temperature and below, the biggest thermal conductivity is observed for $CuInP_2Se_6$ and $AgInP_2S_6$ crystals. The biggest anisotropy of heat transport along and normally to the structural layer is observed for $CuInP_2S_6$

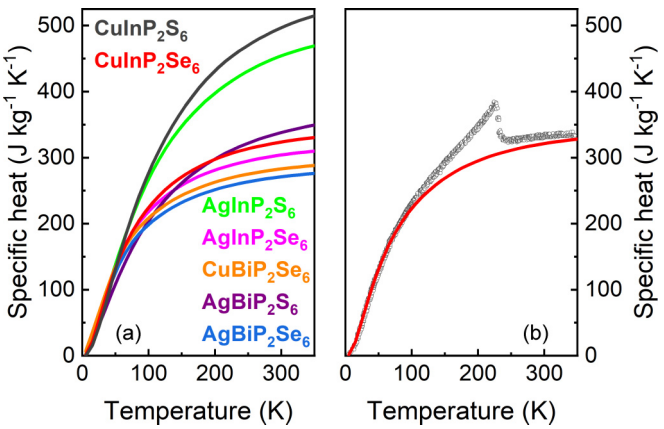

FIG. 4. (a) Calculated specific heat using density-functional perturbation theory for all compounds; (b) comparison of the current calculation (dots) with a published result for $CuInP_2Se_6$ (in red) [28].

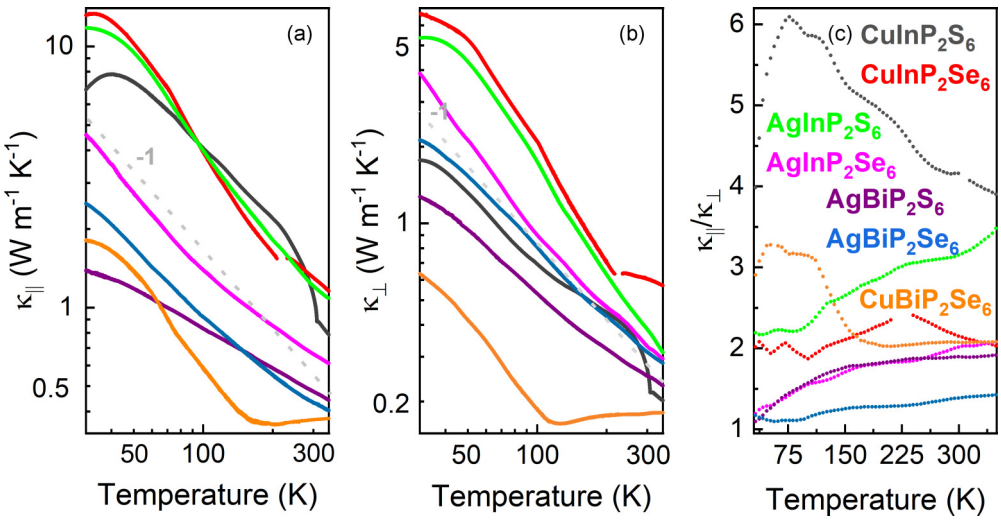

FIG. 5. Thermal conductivity along the layers (a) and perpendicular to them (b) for all layered crystals, where an average T^{-1} law dependence has been added as the grey line; (c) ratio of conductivities, highlighting the thermal anisotropy.

[Fig. 5(c)]. For $CuInP_2Se_6$, $AgInP_2Se_6$ and for all three Bi containing compounds with smaller thermal conductivity at low temperatures, the thermal transfer anisotropy is several times smaller. $AgInP_2S_6$ is an intermediate case in the high temperature region while its thermal anisotropy heavily decreases in the low temperature one.

Thermal conductivity is limited by Umklapp phonon-phonon scattering processes to a value that corresponds to the minimum possible, where the phonon mean-free path (MFP) equals the interatomic distance. In order to check where this situation takes place, the MFP Λ has been calculated using the equations for the lattice thermal conductivity

$$\kappa_L = \tfrac{1}{3} c_v v \Lambda = \tfrac{1}{3} c_v v^2 \tau, \tag{3}$$

where κ_L is the lattice conductivity, C_v is volume heat capacity, v is the average phonon velocity, and τ is the phonon lifetime. The MFP can be extracted as

$$\Lambda = \frac{3D}{v}, \tag{4}$$

where D is the measured thermal diffusivity.

The average phonon velocity can be calculated by the slopes of the three acoustic phonon branches near the Γ point of Brillouin zone taking into account the elastic modulus. The detailed procedure can be found elsewhere [13]. For each direction, the sound velocity is averaged on the two transverse acoustic modes (TA_1 and TA_2) and one longitudinal acoustic mode (LA) by means of the following equation:

$$\frac{3}{v_{\text{average}}^3} = \frac{1}{{v_{TA_1}}^3} + \frac{1}{{v_{TA_2}}^3} + \frac{1}{{v_{LA}}^3}. \tag{5}$$

From the calculated phonon spectra of the investigated compounds, the average sound velocities have been determined for the parallel and normal directions to the structural layers (see Table I), while the mean-free paths have been computed from Eq. (4).

In Figs. 6(a) and 6(b), the mean-free paths at 130 K are compared as a function of T_D. In the case of heat transfer along the layers [Fig. 6(a)] the $\Lambda(T_D)$ dependence is almost linear. In the case of heat transfer in the direction perpendicular to the crystal layers [Fig. 6(b)], only the MFP of $CuInP_2S_6$ deviates off the general linear trend (attaining a lower value), as there is an additional contribution to lattice anharmonicity due to the SOJT effect, which induces the ferrielectric phase transition. In dimensionless coordinates Λ/Λ_D vs T/T_D [Fig. 6(c)], the dependencies for all compounds coincide, corroborating that the Debye temperatures characterize the lattice anharmonicity in $M'M''P_2S(Se)_6$ compounds.

From the presented data, it follows that phonon Umklapp scattering is responsible for the low values of thermal conductivity above T_D, due to the mean-free path approaching the interatomic distance, by intrinsic phonon-phonon processes. At 350 K, for a first group ($AgBiP_2S_6$, $AgBiP_2Se_6$, and $CuBiP_2Se_6$) the thermal conductivity and the phonon MFP (2.8 nm, 2.4 nm, 2.1 nm, respectively, in the layers plane) are extremely low implying that some additional structural disorder exists in this group compared to the rest, especially in the case of $CuBiP_2Se_6$. Another group ($CuInP_2Se_6$ and $AgInP_2S_6$) present higher MFP: 5.2 nm and 6.0 nm, respectively, in the layers plane. $CuInP_2S_6$ does not have a high value of the MFP at 350 K (3.7 nm) but it quickly

TABLE I. Calculated average sound velocities along ($\parallel$) and normal to ($\perp$) the structural layers, Debye frequencies and temperatures determined from the calculated phonon spectra of $M'M''P_2S(Se)_6$ crystals.

Compound	$v_{\text{average}}\parallel$ (m/s)	$v_{\text{average}}\perp$ (m/s)	ω_D (cm^{-1})	T_D (K)
$CuInP_2S_6$	2750	2230	56.4	129
$CuInP_2Se_6$	2680	2330	41.2	94
$AgInP_2S_6$	2360	1600	59.2	135
$AgInP_2Se_6$	2270	1910	35.1	80
$CuBiP_2Se_6$	2280	2140	18.4	42
$AgBiP_2S_6$	2000	1940	36.9	84
$AgBiP_2Se_6$	2160	1830	28.1	64

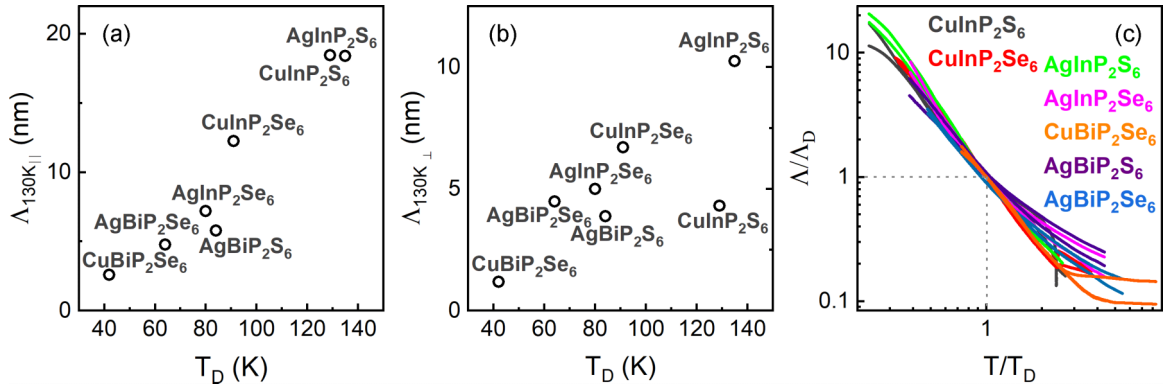

FIG. 6. The mean-free path of heat transferring phonons at 130 K along layers (a) and normal to the layers (b) as a function of T_D. Normalized mean-free path Λ/Λ_D vs normalized temperature T/T_D (c).

grows once the phase transition takes place, on lowering the temperature, joining the previous group. $AgInP_2Se_6$ crystal can be considered as an intermediate case between the more heat conductive and the more resistive groups of compounds, as seen both in κ and the MFP at 350 K (3.6 nm).

At this point, it is interesting to understand why such a big difference exists in the thermal conductivity between $AgInP_2S_6$ and $AgInP_2Se_6$, which is based on the difference in the nature of chemical bonding. In the selenide compound, the relatively low thermal conductivity arises from the lattice vibrations, which create low frequency, localized optical phonons in the acoustic region and thus enable strong anharmonic phonon scattering. Figures 7 and 8 show the calculated phonon dispersions and atom-projected phonon density of states of $AgInP_2S_6$ and $AgInP_2Se_6$ layered crystals. Both compounds share the prominent feature of the presence of low-lying modes, cutting through the acoustic region. For $AgInP_2S_6$, the acoustic modes attain a value slightly higher than $40\,cm^{-1}$ on the edge of the Brillouin zone, and low-energy (near $13\,cm^{-1}$) A_{2g} and A_{2u} symmetry optical phonon modes are found in the acoustic region, both of which are mostly associated with vibrations of Ag atoms normally to the structural layers planes (Fig. 7). At a little higher frequency (near $30\,cm^{-1}$), doubly degenerated E_g symmetry optical modes are also placed, which involve in-plane motions of silver and indium cations together with shifts of $(P_2S_6)^{4-}$ anions. These phonon modes with approximately zero group velocity reflect the locality of vibrations of Ag atoms and confirm the relative weakness of the covalent bonding Ag-S.

In the case of $AgInP_2Se_6$ crystal, the lowest flat optical branches at BZ center have frequencies of $21\,cm^{-1}$ for E_g modes, $29\,cm^{-1}$ for A_{2g} mode and $38\,cm^{-1}$ for B_g mode (Fig. 8). For the selenium compound, the A_g mode frequency increases (from $13\,cm^{-1}$ in $AgInP_2S_6$ crystal to $29\,cm^{-1}$ in $AgInP_2Se_6$) as a result of a bigger covalence of the Ag-Se bonds. Conversely, for the degenerate E_g modes on substitution of S by Se, the frequency decreases from 30 to $21\,cm^{-1}$ as a result of the bigger mass of the $(P_2Se_6)^{4-}$ anions.

In addition to reducing group velocities, the lowest frequency localized optical modes act as scattering centers for low energy acoustic modes. Such resonant scattering further reduces the total lattice thermal conductivity and it is obviously more effective for the selenide crystal, with a bigger polarizability of the heavy $(P_2Se_6)^{4-}$ anions.

In more detail, a larger suppression of κ by the lower flat optical branch energy modes can originate from several reasons. The flat optical branch exhibits an anticrossing with acoustic phonon modes. This largely reduces the group velocity of the heat-carrying acoustic phonons around the optical mode energy, which leads to the suppression of κ. The lower the frequency of the optical mode, the larger the effect, because the group velocity of acoustic phonons is larger at lower energy. The Umklapp scattering that suppresses κ can also be stronger with a lower energy of the optical branch, as lower optical modes must scatter higher acoustic phonons to create the same final phonons. Because acoustic phonons with higher energy have a higher density of states, the Umklapp scattering can be stronger.

Peculiarities of chemical bonding, such as the SOJT effect and the high deformability of the lone-pair electron charge density, can also limit the thermal conductivity in crystalline materials. It has already been shown [29] that in $CuInP_2S_6$ and $CuInP_2Se_6$ compounds the relaxational soft modes appeared due to the SOJT effect with participation of s and d orbitals of Cu^+ cations and p orbitals of $S(Se)^{2-}$ anions. The In^{3+} cations in these ferrielectrics can also be involved in the SOJT effect by hybridization of their s and p electronic orbitals with sulfur or selenium anion p orbitals but indium atoms in these compounds are strongly enough bounded by covalent interaction with the surrounding chalcogenide atoms. Due to the SOJT effect disordering at the transition, heating from the ferrielectric phase into the paraelectric one strongly suppresses the thermal conductivity, what is nicely seen in the case of $CuInP_2S_6$ crystal (Fig. 5).

In the case of $AgInP_2S_6$ and $AgInP_2Se_6$ compounds, the cations Ag^{1+} create stronger covalent bonds inside the chalcogenide octahedra preventing SOJT effect and the transition into a polar state when the temperature is lowered [13]. As was shown above, only for $AgInP_2Se_6$ the strong phonon–phonon interaction is related to the crossing of the low energy optical branch with acoustic branches and therefore κ is reduced to a very low value. But, in $AgBiP_2S_6$ and $AgBiP_2Se_6$ compounds, the physical origin of anharmonicity can also be traced to the existence of the stereochemically active s^2 lone pair of Bi^{3+} cations. The s electron shell of Bi is easily deformed

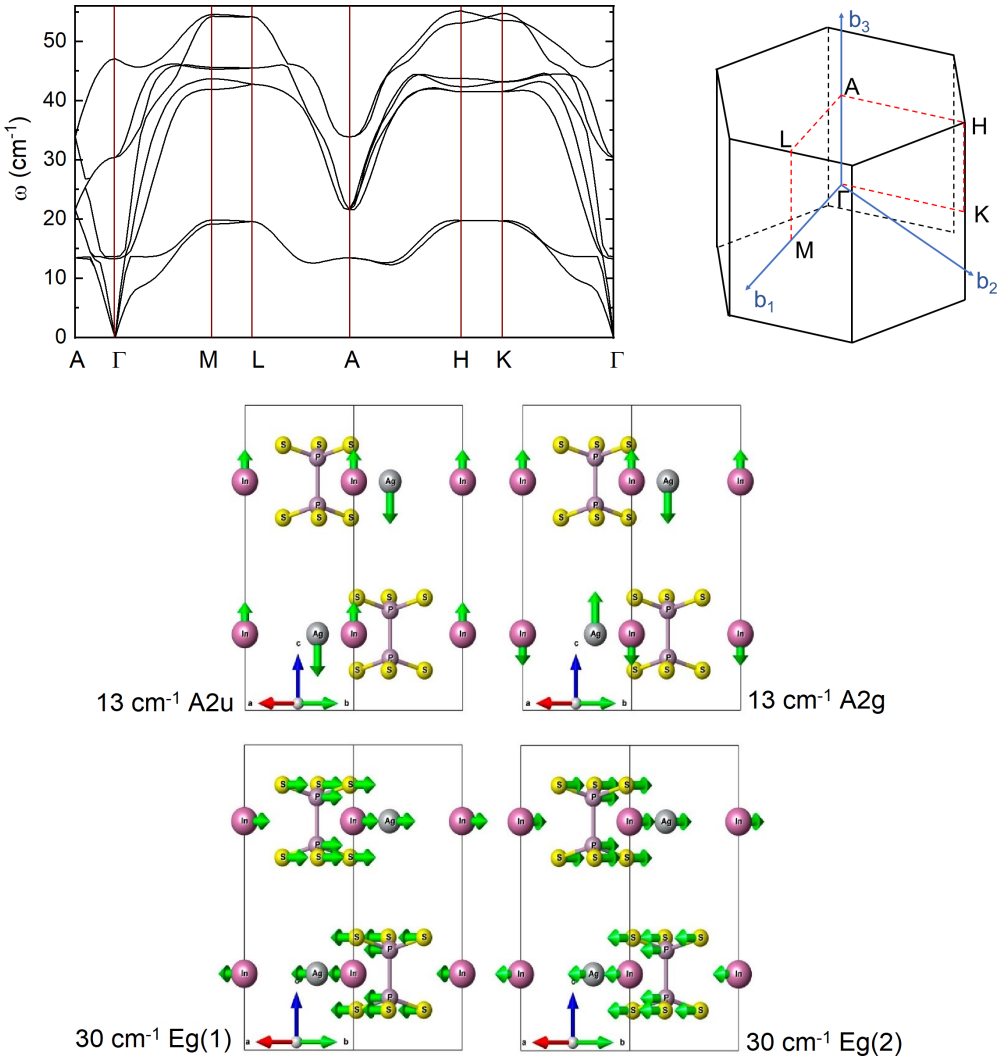

FIG. 7. Phonon spectra of $AgInP_2S_6$ crystal in the low frequency region, with hexagonal Brillouin zone and eigenvectors of lowest energy A_{2g}, A_{2u}, E_g optical modes at BZ center.

by lattice vibrations, resulting in a strong anharmonicity due to the nonlinear terms in the total energy associated with a large electronic response. Obviously, this electron lone pair is also related to the SOJT effect that may lead to the observed structural instability in $CuBiP_2Se_6$ layered crystal [12].

The main idea behind the relationship between an electron lone pair and a low κ is that as atoms approach one another during thermal agitation, the overlapping wave functions of the lone pair and nearby valence electrons will induce a nonlinear repulsive electrostatic force causing increased anharmonicity in the lattice. As the lone pair moves away from the nucleus, anharmonic interactions with adjacent atoms intensify and κ decreases. The highest degree of anharmonicity should thus be achieved when the electron lone pair is far removed from the nucleus, yet not participating in bonding. A similar situation was observed for the $Sn_2P_2S_6$ crystal where Sn^{2+} $5s^2$ lone pair disordering induces the transition from the ferroelectric to the paraelectric phase and effectively suppresses thermal conductivity [48,49].

The electrostatic repulsion between the lone pair electrons and the neighboring chalcogen anions creates anharmonicity in the lattice, the strength of which is determined by the morphology of the lone pair orbital that is illustrated in Fig. 9 for the $AgBiP_2S_6$ layered crystal. It is seen that, as a result of Bi *s* orbitals stereoactivity, the electron density is presented at the top of the valence band in the case of $AgBiP_2S_6$ crystal, but In *s* orbitals electron density is not observed at the top of $AgInP_2Se_6$ valence band. This comparison gives evidence about the hybridization of Bi *s* orbitals with S *p* orbitals and Bi *p* orbitals. Such sp^2 mixing induces the stereoactivity of the Bi s^2 lone pair which appears in the electronic charge space distribution for $AgBiP_2S_6$ crystal, for which Bi *s* orbitals lay in the range (−10.62, −10.49) eV [Fig. 9(d)].

Conversely, the space distribution for In *s* orbitals lying in the energetic range (−6.44, −5.99) eV [Fig. 9(c)] demonstrates their participation in the formation of In–Se covalence bonds.

Finally, we discuss the anomalies in the thermal conductivity temperature dependence related to the structural phase

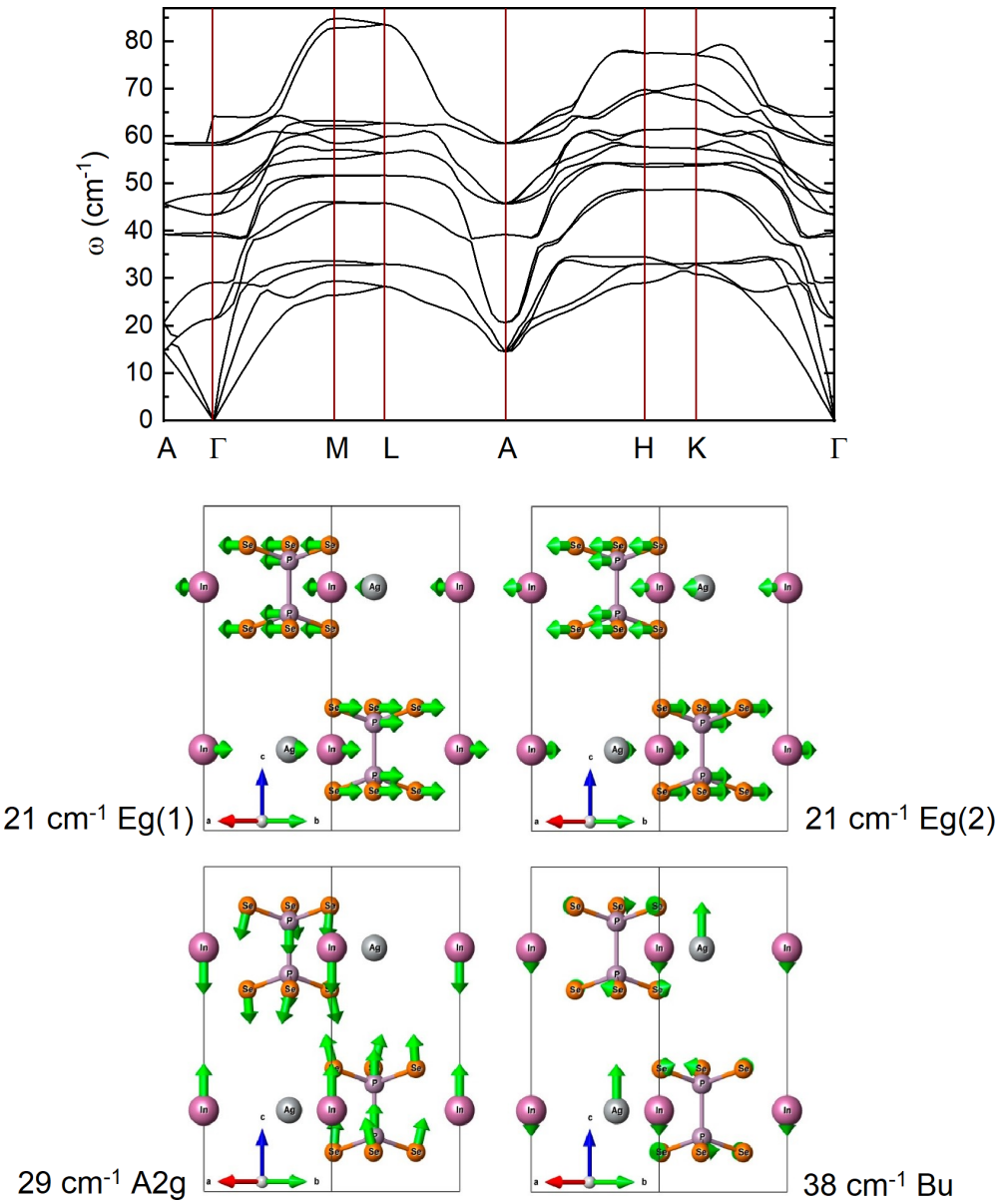

FIG. 8. Phonon spectra of $AgInP_2Se_6$ crystal in the low frequency region with hexagonal Brillouin zone and eigenvectors of lowest energy A_{2g}, A_{2u}, E_g optical modes at BZ center.

transitions. Thermal transport in $CuInP_2S_6$ and $CuInP_2Se_6$ has been previously analyzed in detail [29]. Concerning $CuBiP_2Se_6$, Fig. 5(a) shows that the thermal conductivity of $CuBiP_2Se_6$ along the layers on heating decreases till the minimal value near 200 K. Above this temperature, in the disordered phase, the dependence $\kappa(T)$ demonstrates a glass-sylike behavior. Thermal conductivity normal to the structural layers, while heating, reaches the minimal value already near 100 K—at the transition from the antiferroelectric phase to the intermediate modulated phase [12,30]. The structural modulation of the intermediate phase is oriented normally to the structural layers [12]. So, in the modulated phase, heat transport along the layers is similar to heat transfer in the antiferroelectric phase. Conversely, heat transport normal to the structural layers across the temperature interval of the modulated phase is similar to the observed heat conduction in the disordered high temperature phase.

The reduction of κ in the intermediate modulated phase is probably due to the folding of the Brillouin zone in the direction perpendicular to the structural layers (the direction of the modulation wave vector). Such a suppression of κ has been earlier observed in the incommensurate phase in $Sn_2P_2Se_6$ ferroelectric [8].

IV. CONCLUSIONS

Thermal diffusivity has been measured on single crystals of the layered compounds $Cu_{1-x}Ag_xInP_2(S, Se)_6$ with $x = 0$, 0.1, and 1, $AgBiP_2(S, Se)_6$ and $CuBiP_2Se_6$ in the temperature range 30—350 K, showing important thermal anisotropies, as

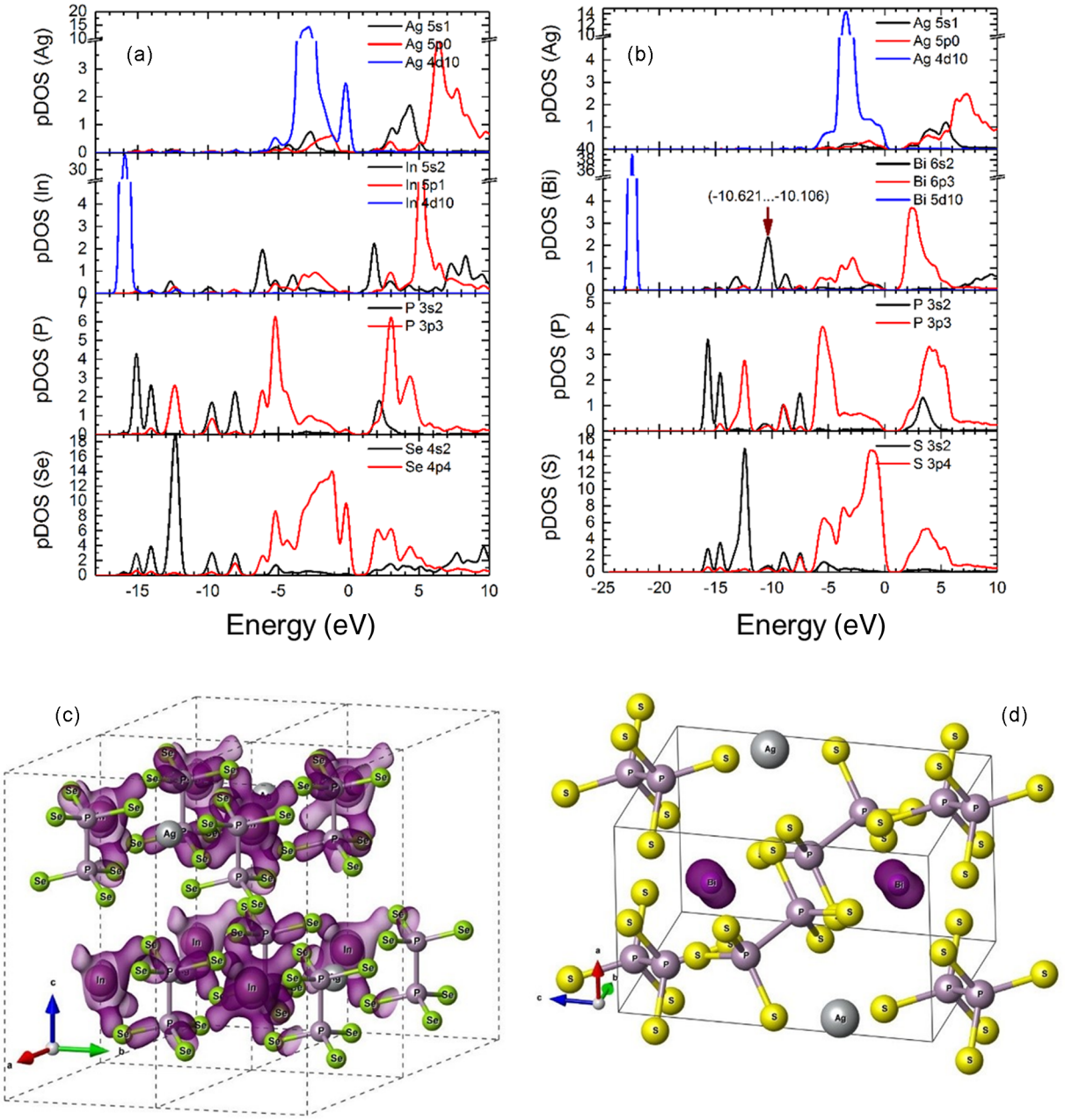

FIG. 9. Partial electron density of states for $AgInP_2Se_6$ (a) and $AgBiP_2S_6$ (b) crystals. Electron density space distribution for orbital laying in the energy range (−6.44, −5.99) eV of $AgInP_2Se_6$ crystal valence band (c), and for orbital laying in the energy range (−10.62, −10.49) eV of $AgBiP_2S_6$ crystal valence band (d).

well as different phase transitions depending on the particular ions present, confirming the different role played by them. Heat capacity has been calculated through the evaluation of the phonon spectra using density-functional perturbation theory, and, through the combination of both variables, thermal conductivity has been obtained in the full temperature range, showing that heat is effectively transferred by phonons and that very low values can be found in several cases due to the enhancement of phonon scattering events, expressing a strong anharmonic behavior, which has been discussed on the basis of disorder, electronic hybridization, the role of lone electron pairs, and the presence or absence of the second-order Jahn-Teller effect.

ACKNOWLEDGMENTS

This work has been supported by Universidad del País Vasco UPV/EHU (Grant No. GIU16/93). V.L. thanks the University of the Basque Country UPV/EHU for his grant under the international cotutelled PhD programme.

[1] M. A. Sussner, M. Chyasnavichyus, M. A. McGuire, P. Ganesh, and P. Maksymovych, Adv. Mater. **29**, 1602852 (2017).

[2] C. Cui, F. Xue, W. J. Hu, and L. J. Li, npj 2D Mater. Appli. **2**, 18 (2018).

[3] F. Wang, T. A. Shifa, P. Yu, P. He, Y. Liu, F. Wang, Z. Wang, X. Zhan, X. Lou, F. Xia, and J. He, Adv. Funct. Mater **28**, 1802151 (2018).

[4] J. R. Reimers, S. A. Tawfik, and M. J. Ford, Chem. Sci. **9**, 7620 (2018).

[5] X. Wang, P. Yu, Z. Lei, C. Zhu, X. Cao, F. Liu, L. You, Q. Zeng, Y. Deng, C. Zhu, J. Zhou, Q. Fu, J. Wang, Y. Huang, and Z. Liu, Nat. Comm. **10**, 3037 (2019).

[6] M. Si, P. Y. Liao, G. Qiu, Y. Duan, and P. D. Ye, ACS Nano **12**, 6700 (2018).

[7] M. Si, A. K. Saha, P. Y. Liao, S. Gao, S. M. Neumayer, J. Jian, J. Qin, N. B. Wisinger, H. Wang, P. Maksymovych, W. Wu, S. K. Gupta, and P. D. Ye, ACS Nano **13**, 8760 (2019).

[8] V. Shvalya, A. Oleaga, A. Salazar, A. A. Kohutych, and Yu.M. Vysochanskii, Mater. Express **7**, 361 (2017).

[9] V. Maisonneuve, V. B. Cajipe, A. Simon, R. Von Der Muhll, and J. Ravez, Phys. Rev. B **56**, 10860 (1997).

[10] R. Pfeiff and R. Kniep, J. Alloy. Comp. **186**, 111 (1992).

[11] Z. Ouili, A. Leblanc, and P. Colombet, J. Solid State Chem. **66**, 86 (1987).

[12] M. A. Gave, D. Bilc, S. D. Mahanti, J. D. Breshears, and M. G. Kanatzidis, Inorg. Chem. **44**, 5293 (2005).

[13] T. Babuka, K. Glukhov, Y. Vysochanskii, and M. Makowska-Janusik, RSC Adv. **8**, 6965 (2018).

[14] V. Maisonneuve, M. Evain, C. Payen, V. B. Cajipe, and P. Molinie, J. Alloy. Comp. **218**, 157 (1995).

[15] Y. Fagot-Revurat, X. Bourdon, F. Bertran, V. B. Cajipe, and D. Malterre, J. Phys.: Condens. Matter **15**, 595 (2003).

[16] V. Samulionis, J. Banys, and Y. Vysochanskii, Ferroelectrics **379**, 69 (2009).

[17] V. Samulionis, J. Banys, A. Dziaugys, M. I. Gurzan, I. P. Pritz, and Y. Vysochanskii, Ferroelectrics **419**, 97 (2011).

[18] J. Banys, J. Macutkevic, V. Samulionis, A. Brilingas, and Yu. Vysochanskii, Phase Transit. **77**, 345 (2004).

[19] J. Macutkevic, J. Banys, R. Grigalaitis, and Yu. Vysochanskii, Phys. Rev. B **78**, 064101 (2008).

[20] J. Macutkevic, J. Banys, and Yu. Vysochanskii, Phys. Stat. Sol. (a) **206**, 167 (2009).

[21] Yu. M. Vysochanskii, V. A. Stephanovich, A. A. Molnar, V. B. Cajipe, and X. Bourdon, Phys. Rev. B **58**, 9119 (1998).

[22] A. Dziaugys, J. Banys, J. Macutkevic, R. Sobiestianskas, and Y. Vysochanskii, Phys. Stat. Sol. (a) **207**, 1960 (2010).

[23] A. Dziaugys, J. Banys, J. Macutkevic, and Yu. Vysochanskii, Ferroelectrics **391**, 151 (2009).

[24] A. Dziaugys, J. Banys, J. Macutkevic, Yu. Vysochanskii, I. Pritz, and M. Gurzan, Phase Transit. **84**, 147 (2011).

[25] A. Galdamez, V. Manriquez, J. Kasaneva, and R. E. Avila, Mat. Res. Bull. **38**, 1063 (2003).

[26] W. Song, R. Fei, and L. Yang, Phys. Rev. B **96**, 235420 (2017).

[27] X. Bourdon, V. Maisonneuve, V. B. Cajipe, C. Payen, and J. E. Fisher, J. Alloy. Comp. **283**, 122 (1999).

[28] K. Moriya, N. Kariya, I. Pritz, Yu. M. Vysochanskii, A. Inaba, and T. Matsuo, Ferroelectrics **346**, 143 (2007).

[29] V. Liubachko, V. Shvalya, A. Oleaga, A. Salazar, A. Kohutych, A. Pogodin, and Yu. M. Vysochanskii, J. Phys. Chem. Solids **111**, 324 (2017).

[30] V. Liubachko, A. Oleaga, A. Salazar, A. Kohutych, K. Glukhov, A. Pogodin, and Yu. M. Vysochanskii, Phase Transit. **92**, 494 (2019).

[31] See Supplemental Material at http://link.aps.org/supplemental/10.1103/PhysRevMaterials.3.104415 for a detailed description of the crystal growth procedure.

[32] A. Altomare, M. C. Burla, M. Camalli, B. Carrozzini, G. L. Cascarano, C. Giacovazzo, A. Guagliardi, A. G. G. Moliterni, G. Polidori, and R. Rizzi, J. Appl. Crystallogr. **32**, 115 (1999).

[33] A. Altomare, C. Cuocci, C. Giacovazzo, A. G.G. Moliterni, R. Rizzi, N. Corriero, and A. Falcicchio, J. Appl. Crystallogr. **46**, 1231 (2013).

[34] V. Shvalya, A. Oleaga, A. Salazar, A. A. Kohutych, and Yu. M. Vysochanskii, Thermochim. Acta **617**, 136 (2015).

[35] X. Gonze, F. Jollet, F. Abreu Araujo, D. Adams, B. Amadon, T. Applencourt, C. Audouze, J. M. Beuken J. Bieder, A. Bokhanchuk, E. Bousquet, F. Bruneval, D. Caliste, M. Côté, F. Dahm, F. Da Pieve, M. Delaveau, M. Di Gennaro, and J. W. Zwanzigerd, Comput. Phys. Commun. **205**, 106 (2016).

[36] W. Kohn and L. J. Sham, Phys. Rev. **140**, A1133 (1965).

[37] J. P. Perdew, K. Burke, and M. Ernzerhof, Phys. Rev. Lett. **77**, 3865 (1996).

[38] S. Grimme, J. Comput. Chem. **27**, 1787 (2006).

[39] H. Monkhorst and J. Pack, Phys. Rev. B **13**, 5188 (1976).

[40] X. Gonze, Phys. Rev. B **55**, 10337 (1997).

[41] C. Lee and X. Gonze, Phys. Rev. B **51**, 8610 (1995).

[42] A. Maradudin, W. Montroll, and H. Weiss *et al.*, *Theory of Lattice Dynamics in the Harmonic Approximation*, 2nd ed. (Academic Press, London, 1971).

[43] S. Wang, Y. Si, J. Yuan, B. Yang, and H. Chen, Phys. Chem. Chem. Phys. **18**, 24210 (2016).

[44] Z. Ma, Z. Guo, H. Zhang, and T. Chang, AIP Advances **7**, 065104 (2017).

[45] B. Moratzavi, M. Makremi, M. Shahrokhi, M. Raeisi, C. V. Singh, T. Rabczuk, and L. F.C. Pereira, Nanoscale **10**, 3759 (2018).

[46] S. Chen, A. Sood, E. Pop, K. E. Goodson, and D. Donadio, 2D Mater. **6**, 025033 (2019).

[47] J. Zhu, T. Feng, S. Mills, P. Wang, X. Wu, L. Zhang, S. T. Pantelides, X. Du, and X. Wang, ACS Appl. Mater. Interfaces **10**, 40740 (2018).

[48] K. Z. Rushchanskii, Y. M. Vysochanskii, and D. Strauch, Phys. Rev. Lett. **99**, 207601 (2007).

[49] K. Glukhov, K. Fedyo, J. Banys, and Y. Vysochanskii, Int. J. Mol. Sci. **13**, 14356 (2012).